On-Chip Electrokinetic Micropumping for Nanoparticle Impact Electrochemistry

Lennart J. K. Weiß[†], Emir Music[†], Philipp Rinklin[†], Marko Banzet[‡], Dirk Mayer[‡], Bernhard Wolfrum[*,†]

[†] Neuroelectronics - Munich Institute of Biomedical Engineering, Department of Electrical Engineering, TUM School of Computation, Information and Technology, Technical University of Munich, Boltzmannstrasse 11, 85748 Garching, Germany

[‡] Institute of Biological Information Processing, Bioelectronics (IBI-3), Forschungszentrum Jülich, 52425 Jülich, Germany

KEYWORDS single-impact electrochemistry, silver nanoparticles, electrokinetic transport, micropumping, electrophoresis, electroosmosis

ABSTRACT: Single-entity electrochemistry is a powerful technique to study interactions of nanoparticles at the liquid-solid interface. In this work, we exploit Faradaic (background) processes in electrolyte of moderate ionic strength to evoke elektrokinetic transport and study its influence on nanoparticle impacts. We implemented an electrode array comprising a macroscopic electrode that surrounds an array of 62 spatially-distributed microelectrodes. This configuration allowed us to alter the global electrokinetic transport characteristics by adjusting the potential at the macroscopic electrode, while we concomitantly recorded silver nanoparticle impacts at the microscopic detection electrodes. By focusing on temporal changes of the impact rates, we were able to reveal alterations in the macroscopic particle transport. Our findings indicate a potential-dependent micropumping effect. The highest impact rates were obtained for strongly negative macroelectrode potentials and alkaline solutions, albeit also positive potentials lead to an increase in particle impacts. We explain this finding by a reversal of the pumping direction. Variations in the electrolyte composition were shown to play a critical role, as the macroelectrode processes can lead to a depletion of ions, which influences both, the particle oxidation and the reactions that drive the transport. Our study highlights that controlled on-chip micropumping is possible, yet its optimization is not straightforward. Nevertheless, the utilization of electro- and diffusiokinetic transport phenomena might be an appealing strategy to enhance the performance of future impact-based sensing applications.

Introduction

Single-entity electrochemistry offers great opportunity to explore physicochemical characteristics at the solid-liquid interface that are typically neglected in mean-field analyses.[1–3] In particular, combined optical-electrochemical and high-resolution recordings from micro- and nanoelectrodes were able to reveal the complexity of nanoparticle (NP) interaction upon collision.[4–11] A key parameter to all impact-electrochemistry studies is the potential at the electrode interface.[12,13] It governs not only the electron-transfer kinetics within the tunneling region but also the particle trajectories in the vicinity of the electrode.[3,14–16] Here, non-negligible Faradaic processes at the electrode establish an electric field in solution and can thereby substantially influence micro- and macroscopic mass transport beyond diffusion. In general, the extend of the electric fields in solution is determined by the ionic strength, since the electrolyte concentration dictates both, the ohmic drop at the electrode as well as the static electrical double layer at dielectric surfaces. Electrokinetic transport becomes increasingly relevant for low-electrolyte conditions but may also affect measurements at moderate ionic strengths.[17] Especially electrophoresis and electroosmosis are two mechanisms that may be primarily considered for a typical (nano-impact) experiment under constant potential control.[18–22] However, the background reaction at the electrode can also drive secondary phenomena, e.g. diffusiophoresis, diffusioosmosis or catalytic micropumping, by altering the electrolyte composition close to the surface.[6,17,23–26] The complex interplay due to an intrinsic coupling by the electrical double layer is most strongly encountered in electrochemical measurements within confined spaces and there have been attempts to facilitate enhanced signal responses via external modulation.[27–31] For instance, Bohn and co-workers investigated the impact of electroosmotic flow and externally-controlled migration on analyte and particle transport within nanopore electrode arrays.[32,33] Likewise, Lemay and co-workers recently studied trajectories of insulating microparticles approaching a biased microelectrode and demonstrated that their motion is dominated by electroosmosis.[21] Although electrokinetic phenomena are proven to play an active role, they are not often utilized in analytical electrochemistry since associated ion migration and electrolysis are typically interfering.[6] However, especially in single-entity electrochemistry it might be an appealing strategy to control the electrokinetic transport, thus, to increase the number of collisions of the species under study.[34] So far, most nanoimpact studies in this regard were carried out at mediator/electrolyte concentrations ≤1 mM and investigated transport that came along with the potential used for detection.[18,21]

Complementary to the existing studies, we investigate the effect of electrokinetic transport at intermediate ionic strength of 25 mM KCl solution. We study the occurrence and shape of

electro-oxidative nanoimpacts of silver nanoparticles (AgNPs) based on parallel recordings from 62 microelectrodes. This enables us to compute ensemble characteristics that reveal information potentially hidden when considering only the motion of single particles.

The experimental control over macroscopic particle transport can be realized by physically decoupling the flow control from particle detection. To this end, we introduce a second macroscopic electrode (ME, with size $1.4\times1.4\,mm^2$) that surrounds the entire microelectrode array (MEA) and is supposed to dominate the macroscopic particle transport via its background reactions. This allows us to manipulate the electrokinetic transport via potential control of the ME while we concomitantly record nanoparticle impacts at the detection electrodes. Previous work reported a positive effect of such a ME via its ability to reduce nanoparticle adsorption typically limiting the performance of surface-based sensors.[35] The goal of the present work is to complement existing studies that focus on electrokinetically-driven particle motion in low-electrolyte solution. We illustrate that, even at moderate ionic strength, electrokinetic processes do play an active role. Moreover, the concept of micropumping that is presented here could find application in digital sensors to enhance the collision rate by simple means.

Experimental Section

Single-Impact Electrochemistry Experiments

The microelectrode array features 62 disk electrodes (8µm in diameter) and a surrounding square electrode with 1.4mm side length, see Fig. S1. The electrodes are made of platinum and the top insulating layer is SiO_2. Further experimental details are provided in the Supporting Information.

Prior to the impact experiments, the chips were electrochemically cleaned in a 4-step routine, which allows multiple usage of the same chip. The status of the electrodes during cleaning was assessed via cyclic voltammetry in mild H_2SO_4 solution (see Fig. S2), which ensures a consistent detection performance for electrodes sharing similar characteristics (see Supporting Information).

The AgNP impact experiments were recorded with a low-noise transimpedance amplifier-system (10 kHz sampling rate per channel, 3.4 kHz bandwidth), which features parallel measurements from 62 detection electrodes in a two-electrode configuration. The potential at the macroscopic electrode (ME) was controlled by an additional potentiostat (VSP-300, BioLogic) in a three-electrode setup. Both systems used the same Ag/AgCl reference electrode, see Supporting Information Fig. S3. If not otherwise stated, 700 µL of 25 mM KCl solution containing 100 pM AgNP (diameter of 20 nm) were used.[35] As previously assessed, particle aggregation was not critical for our conditions.[36] Typically, the ME potential was set to an initial value of -200 mV prior to the AgNP insertion in order to reduce the effect of irreversible adsorption.[35] After 60 s of resting time, the potential at the detection electrodes was stepped to an oxidation potential of 600 mV. While concomitantly recording AgNP impacts, the ME potential was altered to modulate the background reactions which in turn affect the macroscopic transport characteristics.

The detection experiments that were conducted under different step potentials were performed in direct succession with the following order for the ME potential steps: 0 mV, -100 mV, -300 mV, -500 mV, 50 mV, 200 mV, -700 mV, -900 mV, and 600 mV. All experiments with varying supporting electrolyte concentration were also performed in 700 µL solution volume. The alkaline solution (25 mM KCl, pH 9) was prepared by adding additional 5 µL of 100 mM KOH solution.

Data Processing and Analysis

The data was processed in Matlab, similar to a previous study.[35] In short, the analysis includes (i) the rejection of noisy and not well-connected electrodes, (ii) the de-trending of the exponential decay after potential steps, and (iii) a peak-detection method that is based on channel-specific thresholds. To this end, the peak-to-peak noise at 0 mV, i_{pk}, was evaluated for each channel and all current peaks that exceed the limit $0.5\ i_{pk} + 10$ pA were considered as AgNP impacts. Additional to the first current peak, the current traces show subsequent negative peaks (ringing artifacts) introduced by the amplifier system. Therefore, a minimum inter-peak distance of 10 ms was implemented to avoid misclassification. To account for fabrication differences, all further evaluations are based on a reduced dataset created from a subset of channels that typically provided the highest number of AgNP impacts (if not otherwise stated). The analysis for different ME potentials is based on a fixed subset of 18 electrodes containing equal number of inner and outer channels.

Results and Discussion

Externally-Induced Electrokinetic Transport

If we consider a typical nanoimpact experiment, the oxidative dissolution of AgNPs is thermodynamically favored at potentials beyond +200 mV vs. Ag/AgCl in the presence of chloride ions.[37,38] The electrode potential, however, does not only control the reaction of interest but can also influence reactions of other species – in aqueous solutions e.g. the reduction of dissolved oxygen, the onset of metal oxidation, and the electrolysis of water at (higher) potentials.[6,39–41] These interfering Faradaic reactions are commonly ignored, as they only lead to small background currents in most cases. Yet, they cause an electric field in solution and thus unintentionally drive additional mass transport phenomena beyond diffusion.[6,19] For instance, Tarach and co-workers observed a substantial electroosmotic transport generated as a side effect from detection.[20] Furthermore, Lemay and co-workers illustrated the effect of *self-induced* convection on microparticle trajectories in low-electrolyte solutions.[21]

As a complement to these studies, we aim to explore the influence of *externally-induced* electrokinetic transport. We achieve external control by embedding a macroelectrode (ME) – ~38,000 times larger than the microelectrodes, see Fig. 1a and b – that governs the (macroscopic) transport processes; see supplementary videos V1 and V2. Depending on the potential at the ME (with respect to its open circuit potential) and the electrolyte solution, different reactions can be fueled and a background current is induced. In our case of a moderate KCl concentration, we roughly observe negative/positive ME currents for negative/positive ME potentials (see Fig. S4). Thereby, we can expect to induce electric fields that either point towards or away from the ME surface.

The electric field in solution leads to a net force on unbalanced charge densities which can drive particle motion in two different ways – via electrophoresis and/or electroosmosis. Electrophoresis describes the movement of a charged particle due to an electric field in solution. The induced field $\boldsymbol{E}$ can be connected to the average particle velocity $\boldsymbol{v}_{ep}$ via the electrophoretic mobility μ_{ep}

$$\boldsymbol{v}_{\mathrm{ep}} = \mu_{\mathrm{ep}}\boldsymbol{E} \qquad \text{(Eqn. 1)}$$

The relationship between the field and the resulting particle velocity, μ_{ep} is not trivial and challenging to predict, as it critically depends on the radius of the particle r_{p} in relation to the thickness λ of the double layer.[42] Yet, a qualitative picture can be gained by considering limit cases, e.g. a thin electrical double layer compared to the particle size (Smoluchowski approximation). In addition to electrophoresis, the electric field generates as well electroosmotic flows, $\boldsymbol{v}_{\mathrm{eo}}$, by the actuation of the screening ions within the double layer next to the SiO_2-surface. Via viscous interaction, the ionic motion ultimately establishes a 3D flow field. The combination of both effects can be interpreted analogous to a swimmer within a river, where the direction of the carrying solvent flow $\boldsymbol{v}_{\mathrm{eo}}$, might or might not align with the direction of $\boldsymbol{v}_{\mathrm{ep}}$.[23] A quantitative description of the particle flux density is given by an extension of the Nernst-Planck equation, which reads

$$\boldsymbol{j} = \boldsymbol{j}_{\mathrm{d}} + \boldsymbol{j}_{\mathrm{ep}} + \boldsymbol{j}_{\mathrm{eo}} = -D\nabla c + [\boldsymbol{v}_{\mathrm{ep}} + \boldsymbol{v}_{\mathrm{eo}}]c \qquad \text{(Eqn. 2)}$$

with $\boldsymbol{j}$ denoting the particle flux, D the diffusion coefficient, c the particle concentration, and $\boldsymbol{v}_{\mathrm{ep/eo}}$ the particle velocities due to electrophoresis and -osmosis. Depending on the position of the particle, its charge and the surface charge of the passivation, the potential at the ME leads to different outcomes. As shown in Fig. 1c and d, both effects might point in the same or in opposite directions. In our case of negatively charged particles and a negatively charged SiO_2-insulation layer, $\boldsymbol{v}_{\mathrm{ep}}$ and $\boldsymbol{v}_{\mathrm{eo}}$ align in the bulk region but oppose at the chip surface.[43] Moreover, their impact varies with the strength of the electric field in solution, which in turn depends on the background reactions, the electrolyte conductivity, and the cell geometry.

To initially verify our approach of external transport-control, we first studied the trajectories of dielectric microbeads (ζ-potential -9.6±0.2 mV) in deionized water for high ME potentials ranging from -2 V to 2 V. Our results, shown in the supplementary videos V1 and V2, are in line with other work at low ionic strengths,[20,21] as we were able to manipulate the motion of negatively-charged microbeads simply by altering the ME potential (see Fig. S5 and Fig. S6).

The majority of electrochemical analyses operate at moderate electrolyte concentrations. Therefore, it is an interesting question if the previous findings are also applicable in the intermediate to high-electrolyte regime. If so, the integration of a large ME would be an easy-to-implement approach to optimize sensor responses via micropumping. Therefore, we also studied microparticle trajectories within 25 mM KCl for high overpotentials. However, the previous effect was not retained, as ME current densities on the order of 1 µA/cm^2 were not able to visibly govern the microparticles' trajectories. Additionally, changes in the electrical double layers at the particle (ζ-potential at 25 mM KCl -14.3±1.2 mV) and the SiO_2-surface, as well as promoted particle adsorption might alter the influence significantly.[43]

Manipulated AgNP Trajectories

A different, yet indirect approach, to investigate the influence of externally-induced electrokinetic phenomena is by means of single-impact electrochemical recordings instead of optical tracking. In the past, most research concerning this aspect has focused on blocking- or amplifying-impact experiments conducted under low ionic strength.[18,20,21] By far less studied are electrokinetic phenomena at intermediate electrolyte concentrations, although Patel *et al.*[6] as well as Park *et al.*[19] reported significant effects in this regime. Hence, the impact method could potentially be applied to spatially sample the externally-induced flow.

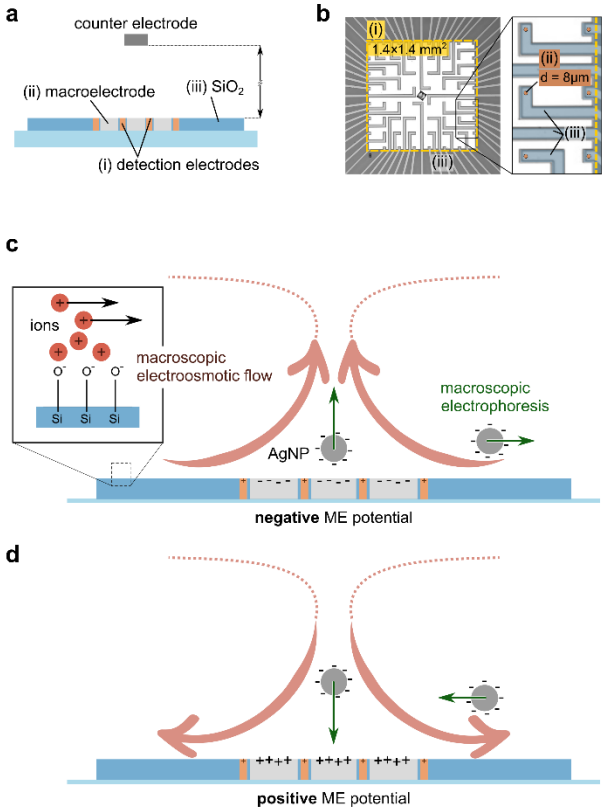

Figure 1 The macroscopic electrokinetic transport is governed by the potential at the ME. (a) Schematic and (b) top-view microscopy image of a MEA chip with a 1.4×1.4 mm^2 large ME (i, yellow) surrounding all detection electrodes. The circular detection electrodes (ii) have a diameter of 8 µm. The feedlines are covered by an insulating SiO_2 surface (iii). Effect of macroscopic electroosmosis and electrophoresis for a negative (c) and a positive (d) potential at the ME. The negative charge at the SiO_2-passivation leads to the formation of an electrical double layer. The accumulated positive charge carriers experience a force due to the electric field from the ME and generate a macroscopic electroosmotic flow. Additionally, an electric force acts on the charged particles causing their electrophoretic attraction for a positive and their repulsion for a negative ME potential.

To test our hypothesis, we conducted a highly-parallelized impact experiment using 100 pM of AgNPs and 25 mM KCl, since nano-impact experiments typically operate in electrolyte concentrations between 20 mM and 50 mM.[37,38,44] The relatively high particle concentration of 100 pM was chosen to continuously yield a high impact rate, whose temporal changes could be directly correlated with variations in the electrokinetic transport. The experiment was performed as follows: We initially applied a potential of -200 mV at the ME and injected the AgNP solution. Then, after a rest time of 60 s, the potential at the detection electrodes was stepped to an oxidation potential of 600 mV and collisions were recorded from 62 electrodes. Concomitantly, the ME potential was altered between -200 mV and -700 mV every 100 s of recording, see Fig. 2a. The current traces from 15 individual electrodes are depicted in Fig. 2b and further statistical data (amplitude, duration, charge, and size distribution) is provided in Fig. S7. Slightly visible in the ensemble data, but more apparent in the zoom-in for channel 1,

the number of impacting particles varies in time. Initially, we observe a decreasing impact rate due to an evolving depletion layer at the vicinity of the electrodes. Afterwards, we find an accumulation of impacts for -700 mV ME potential compared to -200 mV. The effect is repeatable during the application of successive voltage steps, see Fig. 2c and d, and the ensemble average as well as single electrodes follow the same pattern – an increase in the impact rate for -700 mV and a decrease for -200 mV ME potential – although spillover-effects are observed in some channels' data, see e.g. Fig. 2b zoom-in. In principle, there are three phenomena which could support our observations – (i) altered particle adsorption at the ME, (ii) potential-induced transport and (iii) local changes in the electrolyte constitution affecting the oxidation kinetics.

In a previous work, we demonstrated that the adsorption of particles can be reduced via electrostatic repulsion.[35] Consequently, potential changes could modulate the adsorption of AgNPs, and thereby the number of 'accessible' particles during the recording. Assuming a purely diffusive transport ($D = 2.3 \cdot 10^{-11} \mathrm{m}^2/\mathrm{s}$), it would take a particle ~4.5 s to overcome the distance between the ME and a detection electrode. Especially at long recording times, we have to consider the evolution of a depletion layer, which is contradictory to Fig. 2c, where we do not see a diminished influence at longer times. Thus, we conclude that a purely-electrostatic approach oversimplifies the situation, as the steady ME current is non-zero throughout the experiment, see Fig. 2a. In fact, we most likely induce the reduction of dissolved oxygen at the platinum ME[39,40,45]

$$\mathrm{O_2} + 4\mathrm{H^+} + 4e^- \rightarrow 2\mathrm{H_2O}$$

and create an electric field in solution, which potentially drives electrokinetic transport. Once, the electric field distribution is known, the electrokinetic transport could be directly predicted (for the thin-layer limit) via the Helmholtz-Smoluchowski equation,[42] which reads

$$\boldsymbol{v}_{\mathrm{p},\parallel} = \boldsymbol{v}_{\mathrm{ep}} + \boldsymbol{v}_{\mathrm{eo}} = [\mu_{\mathrm{ep}} + \mu_{\mathrm{eo}}]\boldsymbol{E}_{\parallel} = \frac{\epsilon}{\eta}\left(\zeta_{\mathrm{p}} - \zeta_{\mathrm{s}}\right)\boldsymbol{E}_{\parallel} \qquad \text{(Eqn. 3)}$$

where $\boldsymbol{v}_{\mathrm{p},\parallel}$ is the particle velocity close to and in parallel to the dielectric surface, $\boldsymbol{E}_{\parallel}$ is the electric field parallel to the surface, η the viscosity, ϵ the electric permittivity in the solution, and ζ_{p} and ζ_{s} are the ζ-potentials of the particle and at the SiO_2-layer, respectively. However, estimations based on average current densities and conductivities (Ohms law) are misleading, as we expect highly heterogeneous field distributions that are established by induced chemical reactions. Furthermore, as the ME and the detection electrodes have reverse polarities – -200 mV/-700 mV and 600 mV, respectively –, the field establishes not only between the ME and the counter electrode, but also strays towards the detection electrodes. Unfortunately, there is no direct experimental access to the current allocation amongst the CE and detection electrodes, which renders the calculation of the field strength based on experimental data challenging. As Kline *et al.* reported ionic concentration gradients to cause strong local electric fields (in the range of ~ 500 V/m) during catalytic micropumping,[23,46] we assume that the field strength generated in our system is sufficient to drive local electrophoresis and –osmosis. In any case, Eqn. 3 can still be used to estimate the relative importance of both electrokinetic effects. If we only consider particle transport to be the origin for the results in Fig. 2, we have to conclude that the transport must be dominated by lateral electroosmosis, since we observe an increase in impacts although the negatively-charged particles are expected to be pushed outwards by electrophoresis (see Fig. 1c). Although Eqn. 3 is not fully applicable for a Debye length of ~2 nm and a particle radius of 10 nm, its prediction of predominant electroosmosis ($\zeta_{\mathrm{p}} = -45.7 \pm 2.2$ mV for of 25 mM KCl at pH 6, $\zeta_{\mathrm{s}} \approx -60$ mV at pH 6[43]) matches well with our findings. We performed numerical simulations in a simplified 2D-band electrode geometry that captures only major interdependencies of the chip geometry and focuses on primary effects. The results, see Fig. S8, support our hypothesis of predominant electroomosis and an externally-evoked pumping effect. Remarkably, the numerical results did not only indicate the presence of a macroscopic rotational flow field, as depicted in Fig. 1c and d, but also the existence of smaller vortices induced by the SiO_2-surface around the detection electrodes.

Last, the continuous current at the ME does additionally modify the electrolyte constitution close to the detection electrodes. As H^+ ions are consumed during the oxygen reduction reaction, we (unintentionally) manipulate the local pH-value and could thereby also alter the reaction kinetics at the detection electrodes. The depletion of H^+ ions shifts the local pH-value towards higher values and alkaline solutions were recently shown to enhance the detection rate of AgNPs.[3,47–51] A second, yet often overlooked phenomena, is also associated with the local Faradaic reactions, since they establish a persistent concentration gradient of electrolytic ions. In our case, the local depletion of H^+ ions at the ME and the generation of H^+ ions at the detection electrodes (during water oxidation at the platinum surface) establishes a H^+ gradient and could, thus, induce associated diffusiokinetic transport. In fact, Kanoufi and colleagues[6], proposed in an experiment comparable to ours diffusiophoresis to be responsible for the propelling of particles that are close to a polarized electrode. In other research, solute concentration gradients were reported to be the origin of a plethora of fascinating phenomena, for instance of self-propelling Janus swimmers or the levitation or separation of particles in solution, yielding diffusiokinetic velocities in the range of several 10 µm/s.[23,52–57] However, predicting the (electro-)diffusiokinetic effects is more subtle as for electrokinetic transport, especially if charged species are generated or consumed. Then, both phenomena, the electrokinetic and diffusiokinetic transport, become deeply coupled, which can lead to highly nonlinear behavior.[58–65] Therefore, it is not possible to separate both mechanisms and distinguish their isolated contributions to the particle transport. Based on our experimental findings, we hypothesize an externally-induced surface-driven net transport towards the sensing area and conclude that the lateral particle supply must overcompensate the electrophoretic repulsion. Then, the increase in AgNP impacts for more negative ME potentials might be attributed to the higher electric potential and the stronger H^+-gradient tangential to the SiO_2-surface, both enhancing their convective contributions.

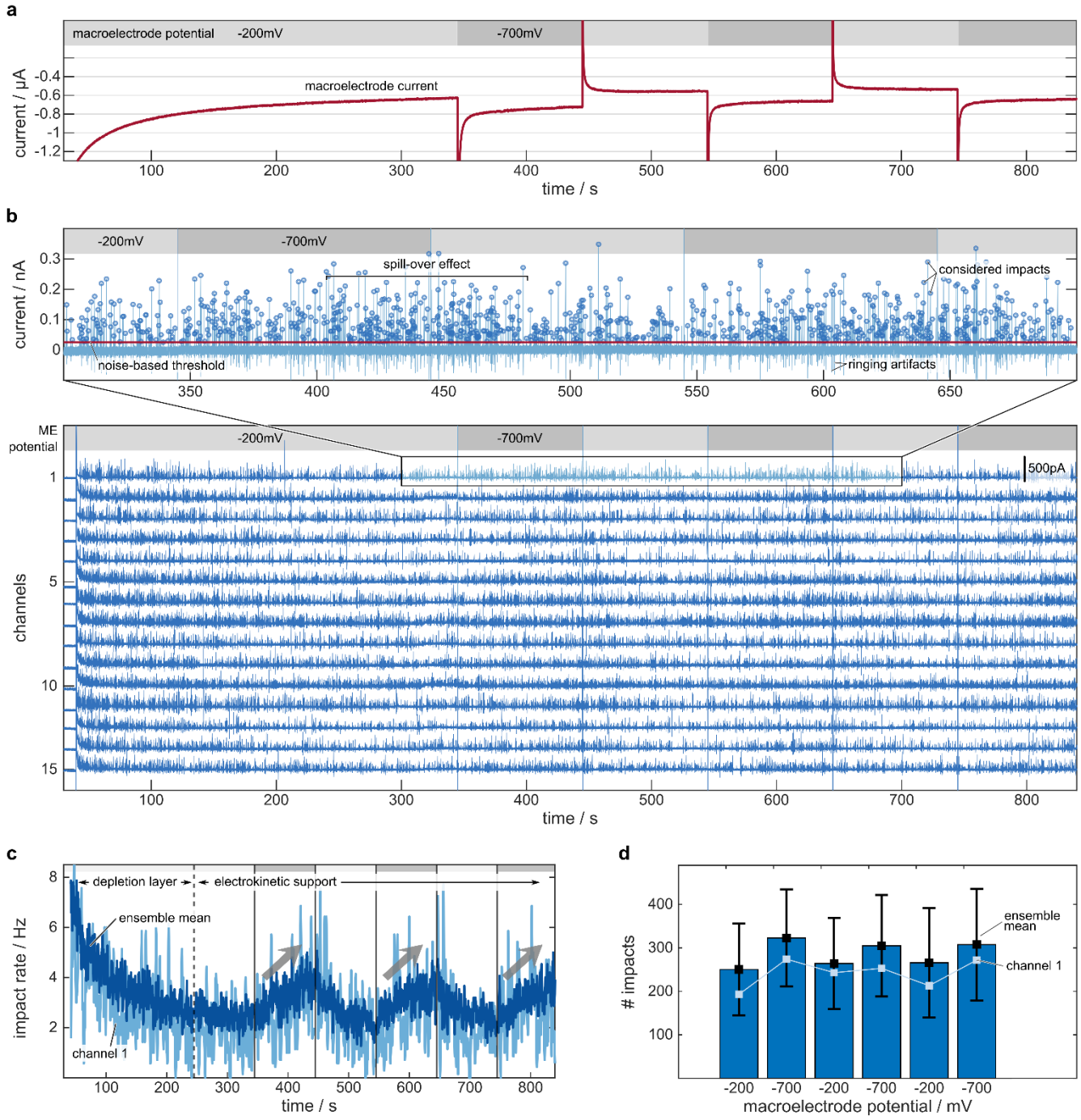

Figure 2 AgNP detection under externally-induced micropumping. The potential at the ME manipulates the number of AgNP impacts on the detection electrodes. (a) Current at the ME while the ME potential is stepped between -200mV and -700mV vs. Ag/AgCl. (b) Current traces from 15 detection electrodes (showing highest number of impacts) in case of 100 pM AgNPs in 25mM KCl. The zoom-in exemplarily depicts the channel-specific current threshold and current peaks considered for further analysis. The effect of an altered ME potential is visible, although there might be spill-over effects. Note, the negative current spikes stem from amplifier-related artifacts that follow the initial charge injection. (c) Temporal evolution of the impact rate. The data is based on the electrodes shown in (b). (d) Number of impacts according to the ME potential. The graph shows the ensemble means and error bars indicate standard deviations. The analysis considers only particle impacts occurring after the initial depletion ($t > 250$ s).

In terms of absolute values, however, the impact rates in Fig. 2c are at all times substantially lower than expected.[66] For instance, if we assume a purely diffusive transport and a reflecting boundary, the impact rate should be ~21 Hz according to Shoup Szabo.[67] Intuitively, one would consider even higher rates in case of additional advection. Yet, this reasoning is only valid for an instantaneous reaction upon collision with the microelectrode – which is only an ideal case and typically not supported by experimental data.[68,69] Moreover, particle adsorption and aggregation, as well as, electrode contamination and particle impurities play a critical role and lower the detection yield.[7,35,44]

If lateral motion primarily rules the AgNP transport, we would expect that the impact rate is dependent on the electrode position within the ME. Indeed, Fig. 3 illustrates such an effect. Here, we altered the ME potential (between -200 mV and

0 mV) and observed a significantly different response at different electrode locations, see Fig. 3b and c. There are effectively two subsets of electrodes showing congruent responses. In general, outer electrodes could detect approximately twice as many AgNPs as inner ones. Moreover, a change in ME potential is well reflected in the impact rate at outer but barely visible at the inner electrodes, see Fig. 3b. To our surprise, the detected sizes also vary slightly, with the outer electrodes detecting supposedly larger particles, see Fig. 3d. A statistical analysis, see Fig. S6, reveals lower amplitudes and an increased duration for impacts at the inner electrodes, which might stem from a reduced influx of chloride ions during the oxidation.[38] We find further evidence for our hypothesis, since more negative ME potentials also lead to smaller and slightly longer impacts (see data for -200mV and 0mV in Fig. S9). A possible explanation could be the accompanying depletion of chloride ions via electrophoresis. Interestingly, Saw *et al*. reported similar observations – lower amplitude, extended duration of the current spike – for particle detection in water-alcohol mixtures. They likewise attribute the phenomenon to an impaired diffusive anion flux due to the presence of bulkier alcohol molecules in the solvation shell of the anion.[70]

Influence of the Potential at the Macroelectrode

In the next experiment, we studied the influence of different ME potentials on the detection rate. Here, we chose a common potential of -200 mV at the beginning and at the end of each experiment to ensure similar conditions regarding adsorption and convection throughout the study. The temporal evolution of the impact rate (Fig. 4a) and the exemplary current traces (Fig. 4b) show an interesting trend. Moderate potentials between -300 mV and 50 mV did not significantly alter the general trend of the impact rate (within the chosen experimental time). Beyond this range, however, we observed two robust characteristics. Negative ME potentials caused a significant increase in impacts and the effect roughly scales with the current at the ME, see Fig. 4c. The ME current is mainly driven by the reduction of dissolved oxygen at moderate potentials. In case of -900mV, however, we observed a drastic increase in the ME current, as well as the impact rate, which we attributed to the onset of the hydrogen evolution reaction. A closer look at the raw data in Fig. 4b illustrates also spillover-effects from one condition to the other, which we associate to inertial forces that tend to continue the previously evoked flow field. Both findings are in line with a macroscopic surface-driven convection as a major driving mechanism. Unexpectedly, more positive ME potentials also lead to increased impact rates. This is surprising, since for potentials above ~200 mV vs. Ag/AgCl the ME acts as particle sink depleting the microenvironment at the detection electrodes. The oxidation current at the ME indicates a reverse flow direction (see Fig. 1d) in these cases. Hence, the convective supply and electrophoretic attraction from the bulk solution seem to (over)compensate the loss of particles due to oxidation at the ME. This hypothesis is supported by the drop in impact rate after stepping back from a positive ME potential to -200mV. We attributed this drop to a depletion of AgNPs in the bottom layers, which becomes apparent after reverting the flow field. The depletion for positive ME potentials is also location-dependent, see Fig. S10. Again, we observed a stronger response at outer electrodes which can be explained by the establishing flow field and a ME that competes with the inner electrodes for particle detection.

In summary, the results in Fig. 4 illustrate the possibility to modulate AgNP trajectories by a macroscopic electrode. Moreover, we could clearly demonstrate the active role of background reactions driving the electrokinetic transport. Its impact, however, varies with the strength and direction of the electric field as well as the measurement time.

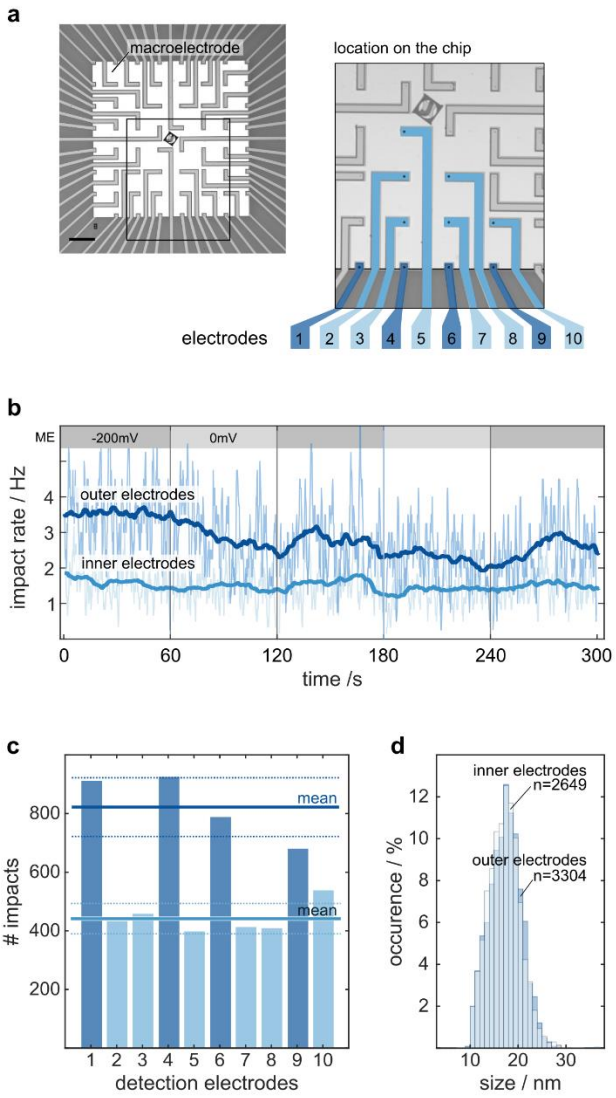

Figure 3 Position-dependent impact rates. The position of the detection electrode determines its response to different ME potentials. Lateral surface-driven flow leads to an increased detection rate at the outer electrodes. (a) Position of the detection electrodes on the chip. (b) Mean temporal evolution of the impact rate for the ensembles of inner and outer electrodes. (c) Number of detected peaks during the experiment. (d) Particle size distribution according to the electrode position. The distribution is calculated from all impacts at all electrodes.

Effect of the Electrolyte Composition

Our results indicate a strong dependence on the electrolyte composition as both, the electrolyte and the ME potential, govern the electric field in solution. The electrolyte does not only affect the background reactions at the ME but also the reaction kinetics at the detection electrode. In fact, both the oxygen reduction reaction and the AgNP oxidation were reported to be enhanced within alkaline media, most probably due to a reduced adsorption energy and a promoted dissolution of AgCl.[3,40] Therefore, we wanted to test if a higher pH yields a more efficient transport and performed single-step experiments

in 25 mM KCl at pH 6 and pH 9, as shown in Fig. 5. The results are in line with our expectations and highlight the critical role of the electrolyte composition. For instance, the impact rate at pH 9 was higher than at pH 6 for all times. However, the drastic increase at pH 9 in case of -700 mV ME potential and its further stabilization around 6 Hz were unexpected, as the particle ζ-potentials (-46±2 mV for 25 mM KCl at pH 6 and -41±2 mV at pH 9) as well as the ME currents were in a similar range for both pH values, see Fig. 5b. Therefore, we associate the enhancement also with an increased negative ζ-potential of the chip wall, rendering the surface-driven convection more effective.[43] The strong positive effect diminishes after releasing the potential at the ME.

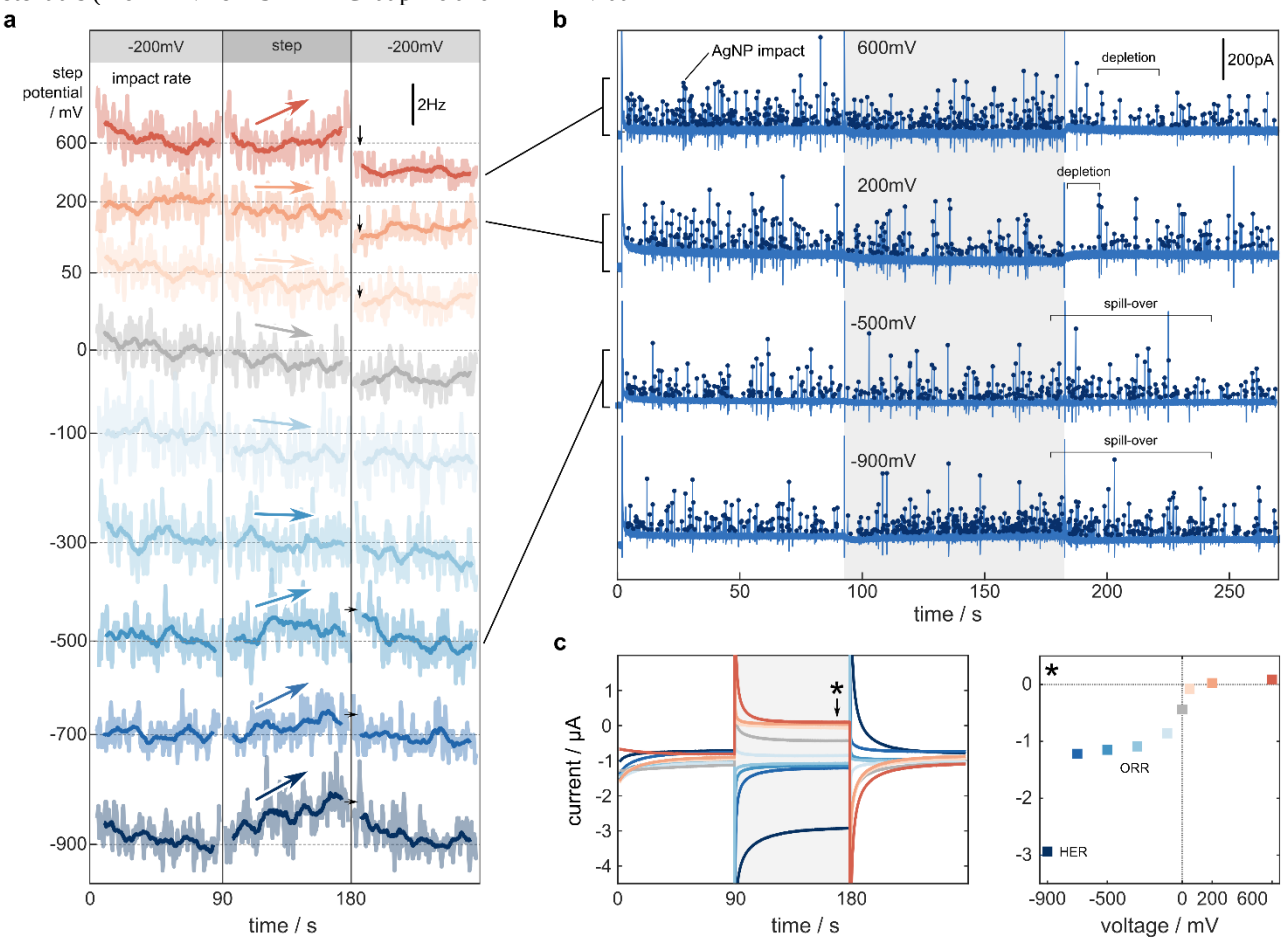

Figure 4 Influence of the potential at the ME on AgNP impacts at the detection electrodes. Background reactions at the ME determine the direction and strength of the potential an ionic gradients in solution, which govern the electro- and diffusiokinetic transport. (a) Mean temporal evolution of the impact rate for different step potentials at the ME. The data is based on a subset of 9 inner and 9 outer detection electrodes. (b) Exemplary current traces that illustrate depletion effects for positive ME potentials and spill-over effects at negative ME potentials. (c) Current at the ME for all experiments shown in (a). Oxygen reduction (ORR) determines the current for moderate negative potentials, whereas the current for -900mV is dominated by the hydrogen evolution (HER).

This finding is supported by the control measurements in Fig. 5c, where we recorded impacts while the ME potential was floating. The effect of pH on the impact rate is rather subtle in this case, but persisted for longer measurement times. The data indicates that the alkaline solution leads to a stabilization of the impact rate for longer times which might be associated with a promoted dissolution of AgO_x in alkaline solutions. Yet, we could not observe other features attributed to AgO_x formation upon impact, like extended current tails, which Ma *et al.* recently reported.[3]

Our results indicate that the ME notably affects the distribution of chloride ions in solution. Further step experiments at different electrolyte concentrations – 20 mM and 30 mM KCl, see Fig. S11 – confirmed this, as the outcome varied significantly for the two different chloride concentrations. Our results highlight that negative ME potentials impairs the chloride flux to a point such that the initial detection rate might be significantly reduced compared to moderate potentials. In fact, other recent work highlights the crucial role of the co-reactants in impact-experiments, as the reaction dynamics are very sensitive to the presence/absence of the co-species at the electrode.[71,72]

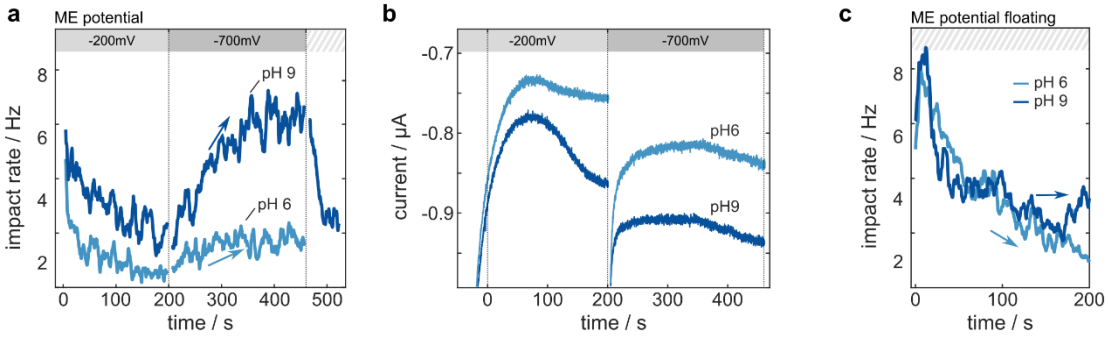

Figure 5 Effect of an alkaline electrolyte solution on the electrokinetic transport of AgNPs. There is a substantial enhancement of the impact rate at pH 9. (a) Temporal evolution of the impact rate for different pH values in case of a ME potential step from -200 mV to -700 mV. (b) Current at the ME reflecting the background reactions at different pH. (c) Control experiment, where the ME was not under potentiostatic control.

Conclusion and Outlook

In conclusion, we demonstrated the possibility to modulate nanoparticle trajectories via micropumping induced by a ME that controls the microenvironment around the detection electrodes. The background reactions lead to an electric field and an ionic gradient in solution that induce externally-controlled convection and electro-/diffusiophoretic motion. The combined effect acting on the particle is highly position-dependent since the convective flow field establishes a vortex that points upwards above the center of the ME for negative potentials.

The ME potential is able to revert the flow direction and, thus, to convectively supply particles either from the surrounding area close to the passivation surface – indicated by negative ME currents – or from the bulk – for positive ME currents. Interestingly, we found in both cases an increase in AgNP impacts for high potentials, although the effect was strongest for -900 mV ME potential, most likely due to the onset of the hydrogen evolution reaction. The influence of micropumping is also not uniform across the electrode ensemble. At negative potentials, we observed higher impact rates at electrodes that were located at the boundary of the ME, which indicates the surface-driven transport (e.g. electroosmosis) to be dominant. As both, the potential and the electrolyte, govern the pumping-effect, this strategy could be appealing to optimize the mass transport by an elaborate sensor design and a careful selection of the electrolyte. Indeed, we could demonstrate that the impact rate drastically increases for experiments in alkaline solutions. However, the externally-induced transport might also introduce interfering effects that thwart higher impact rates, e.g. due to a depletion of co-reactants. Thus, we conclude that designing electrokinetic transport with the aim of an enhanced impact rate is challenging and requires the consideration of several interdependent processes. Here, in-depth numerical simulations might help in the design process.

Nevertheless, we provided evidence that electrokinetic transport can play an active role in impact electrochemistry experiments, even at moderate ionic strengths. With our highly parallel recordings, we were able to investigate the phenomena under conditions typical in analytical and impact electrochemistry. Thus, the framework of a decoupled transport-control and parallelized detection could be an interesting approach to study further transport phenomena as well as a promising engineering strategy for future ultra-sensitive digital sensors.

SUPPORTING INFORMATION CONTENT

Additional details are provided as mentioned below:

- Details concerning the MEA chips, the cleaning routine and the experimental setup
- Video recording V1 and V2 of negatively-charged microparticles driven by the potential at a ME in the absence of a supporting electrolyte.
- Cyclic voltammetry in 25mM KCl at different pH values
- Statistical data including amplitude, duration and charge distributions for impact experiments shown in the manuscript.
- Potential and velocity distributions for a simplified 2D band-electrode geometry obtained from finite-element simulations.
- Effect of electrode location for step experiments with positive ME potentials
- Results for step experiments with different KCl concentrations

AUTHOR INFORMATION

Corresponding Author

* Bernhard Wolfrum, Neuroelectronics - Munich Institute of Biomedical Engineering, Department of Electrical Engineering, TUM School of Computation, Information and Technology, Technical University of Munich, Boltzmannstrasse 11, 85748 Garching, Germany, bernhard.wolfrum@tum.de

Author Contributions

L.J.K.W., P.R. and B.W. designed the experimental outline. M.B. fabricated the MEA devices. L.J.K.W and E.M. performed the experiments. L.J.K.W. wrote the manuscript with support from P.R., D.M. and B.W.

Funding Sources

The authors received funding from the German Research Foundation (DFG, grant number WO 1510/7-1).

Notes

The authors declare no competing financial interest.

ACKNOWLEDGMENT

The authors thank H. Url for help during the experimental procedure. The authors acknowledge support from N. Wolters regarding the detection device.

REFERENCES

(1) Xu, W.; Zou, G.; Hou, H.; Ji, X. Single Particle Electrochemistry of Collision. *Small* **2019**, *15* (32), 1804908. https://doi.org/10.1002/smll.201804908.

(2) Brasiliense, V.; Patel, A. N.; Martinez-Marrades, A.; Shi, J.; Chen, Y.; Combellas, C.; Tessier, G.; Kanoufi, F. Correlated Electrochemical and Optical Detection Reveals the Chemical Reactivity of Individual Silver Nanoparticles. *J. Am. Chem. Soc.* **2016**, *138* (10), 3478–3483. https://doi.org/10.1021/jacs.5b13217.

(3) Ma, H.; Chen, J.-F.; Wang, H.-F.; Hu, P.-J.; Ma, W.; Long, Y.-T. Exploring Dynamic Interactions of Single Nanoparticles at Interfaces for Surface-Confined Electrochemical Behavior and Size Measurement. *Nature Communications* **2020**, *11* (1), 2307. https://doi.org/10.1038/s41467-020-16149-0.

(4) Ustarroz, J.; Kang, M.; Bullions, E.; Unwin, P. R. Impact and Oxidation of Single Silver Nanoparticles at Electrode Surfaces: One Shot versus Multiple Events. *Chem. Sci.* **2017**, *8* (3), 1841–1853. https://doi.org/10.1039/C6SC04483B.

(5) Oja, S. M.; Robinson, D. A.; Vitti, N. J.; Edwards, M. A.; Liu, Y.; White, H. S.; Zhang, B. Observation of Multipeak Collision Behavior during the Electro-Oxidation of Single Ag Nanoparticles. *J. Am. Chem. Soc.* **2017**, *139* (2), 708–718. https://doi.org/10.1021/jacs.6b11143.

(6) Patel, A. N.; Martinez-Marrades, A.; Brasiliense, V.; Koshelev, D.; Besbes, M.; Kuszelewicz, R.; Combellas, C.; Tessier, G.; Kanoufi, F. Deciphering the Elementary Steps of Transport-Reaction Processes at Individual Ag Nanoparticles by 3D Superlocalization Microscopy. *Nano Lett.* **2015**, *15* (10), 6454–6463. https://doi.org/10.1021/acs.nanolett.5b02921.

(7) Sundaresan, V.; Monaghan, J. W.; Willets, K. A. Visualizing the Effect of Partial Oxide Formation on Single Silver Nanoparticle Electrodissolution. *J. Phys. Chem. C* **2018**, *122* (5), 3138–3145. https://doi.org/10.1021/acs.jpcc.7b11824.

(8) Fosdick, S. E.; Anderson, M. J.; Nettleton, E. G.; Crooks, R. M. Correlated Electrochemical and Optical Tracking of Discrete Collision Events. *J. Am. Chem. Soc.* **2013**, *135* (16), 5994–5997. https://doi.org/10.1021/ja401864k.

(9) Lemineur, J.-F.; Noël, J.-M.; Courty, A.; Ausserré, D.; Combellas, C.; Kanoufi, F. In Situ Optical Monitoring of the Electrochemical Conversion of Dielectric Nanoparticles: From Multistep Charge Injection to Nanoparticle Motion. *J. Am. Chem. Soc.* **2020**, *142* (17), 7937–7946. https://doi.org/10.1021/jacs.0c02071.

(10) Hao, R.; Fan, Y.; Zhang, B. Imaging Dynamic Collision and Oxidation of Single Silver Nanoparticles at the Electrode/Solution Interface. *J. Am. Chem. Soc.* **2017**, *139* (35), 12274–12282. https://doi.org/10.1021/jacs.7b06431.

(11) Ma, C.; Wu, W.; Li, L.; Wu, S.; Zhang, J.; Chen, Z.; Zhu, J.-J. Dynamically Imaging Collision Electrochemistry of Single Electrochemiluminescence Nano-Emitters. *Chemical Science* **2018**, *9* (29), 6167–6175. https://doi.org/10.1039/C8SC02251H.

(12) Peljo, P.; Manzanares, J. A.; Girault, H. H. Variation of the Fermi Level and the Electrostatic Force of a Metallic Nanoparticle upon Colliding with an Electrode. *Chem. Sci.* **2017**, *8* (7), 4795–4803. https://doi.org/10.1039/C7SC00848A.

(13) Lu, S.-M.; Chen, J.-F.; Peng, Y.-Y.; Ma, W.; Ma, H.; Wang, H.-F.; Hu, P.; Long, Y.-T. Understanding the Dynamic Potential Distribution at the Electrode Interface by Stochastic Collision Electrochemistry. *J. Am. Chem. Soc.* **2021**. https://doi.org/10.1021/jacs.1c02588.

(14) Ma, W.; Ma, H.; Yang, Z.-Y.; Long, Y.-T. Single Ag Nanoparticle Electro-Oxidation: Potential-Dependent Current Traces and Potential-Independent Electron Transfer Kinetic. *J. Phys. Chem. Lett.* **2018**, *9* (6), 1429–1433. https://doi.org/10.1021/acs.jpclett.8b00386.

(15) Chung, H. J.; Lee, J.; Hwang, J.; Seol, K. H.; Kim, K. M.; Song, J.; Chang, J. Stochastic Particle Approach Electrochemistry (SPAE): Estimating Size, Drift Velocity, and Electric Force of Insulating Particles. *Anal. Chem.* **2020**, *92* (18), 12226–12234. https://doi.org/10.1021/acs.analchem.0c01532.

(16) Ma, W.; Ma, H.; Chen, J.-F.; Peng, Y.-Y.; Yang, Z.-Y.; Wang, H.-F.; Ying, Y.-L.; Tian, H.; Long, Y.-T. Tracking Motion Trajectories of Individual Nanoparticles Using Time-Resolved Current Traces. *Chem. Sci.* **2017**, *8* (3), 1854–1861. https://doi.org/10.1039/C6SC04582K.

(17) Chinappi, M.; Yamaji, M.; Kawano, R.; Cecconi, F. Analytical Model for Particle Capture in Nanopores Elucidates Competition among Electrophoresis, Electroosmosis, and Dielectrophoresis. *ACS Nano* **2020**, *14* (11), 15816–15828. https://doi.org/10.1021/acsnano.0c06981.

(18) Boika, A.; Thorgaard, S. N.; Bard, A. J. Monitoring the Electrophoretic Migration and Adsorption of Single Insulating Nanoparticles at Ultramicroelectrodes. *J. Phys. Chem. B* **2013**, 10.

(19) Park, J. H.; Boika, A.; Park, H. S.; Lee, H. C.; Bard, A. J. Single Collision Events of Conductive Nanoparticles Driven by Migration. *J. Phys. Chem. C* **2013**, *117* (13), 6651–6657. https://doi.org/10.1021/jp3126494.

(20) Thorgaard, S. N.; Jenkins, S.; Tarach, A. R. Influence of Electroosmotic Flow on Stochastic Collisions at Ultramicroelectrodes. *Anal. Chem.* **2020**, *92* (18), 12663–12669. https://doi.org/10.1021/acs.analchem.0c02889.

(21) Moazzenzade, T.; Yang, X.; Walterbos, L.; Huskens, J.; Renault, C.; Lemay, S. G. Self-Induced Convection at Microelectrodes via Electroosmosis and Its Influence on Impact Electrochemistry. *J. Am. Chem. Soc.* **2020**, *142* (42), 17908–17912. https://doi.org/10.1021/jacs.0c08450.

(22) Boika, A.; Bard, A. J. Electrophoretic Migration and Particle Collisions in Scanning Electrochemical Microscopy. *Anal. Chem.* **2014**, *86* (23), 11666–11672. https://doi.org/10.1021/ac502944n.

(23) Kline, T. R.; Paxton, W. F.; Wang, Y.; Velegol, D.; Mallouk, T. E.; Sen, A. Catalytic Micropumps: Microscopic Convective Fluid Flow and Pattern Formation. *J. Am. Chem. Soc.* **2005**, *127* (49), 17150–17151. https://doi.org/10.1021/ja056069u.

(24) Contento, N. M.; Bohn, P. W. Tunable Electrochemical PH Modulation in a Microchannel Monitored via the Proton-Coupled Electro-Oxidation of Hydroquinone. *Biomicrofluidics* **2014**, *8* (4), 044120. https://doi.org/10.1063/1.4894275.

(25) Contento, N. M.; Bohn, P. W. Electric Field Effects on Current–Voltage Relationships in Microfluidic Channels Presenting Multiple Working Electrodes in the Weak-Coupling Limit. *Microfluid Nanofluid* **2015**, *18* (1), 131–140. https://doi.org/10.1007/s10404-014-1424-9.

(26) McPherson, I. J.; Brown, P.; Meloni, G. N.; Unwin, P. R. Visualization of Ion Fluxes in Nanopipettes: Detection and Analysis of Electro-Osmosis of the Second Kind. *Anal. Chem.* **2021**, *93* (49), 16302–16307. https://doi.org/10.1021/acs.analchem.1c02371.

(27) Fan, L.; Liu, Y.; Xiong, J.; White, H. S.; Chen, S. Electron-Transfer Kinetics and Electric Double Layer Effects in Nanometer-Wide Thin-Layer Cells. *ACS Nano* **2014**, *8* (10), 10426–10436. https://doi.org/10.1021/nn503780b.

(28) Kostiuchenko, Z. A.; Cui, J. Z.; Lemay, S. G. Electrochemistry in Micro- and Nanochannels Controlled by Streaming Potentials. *J. Phys. Chem. C* **2020**, *124* (4), 2656–2663. https://doi.org/10.1021/acs.jpcc.9b08584.

(29) Ma, C.; Xu, W.; Wichert, W. R. A.; Bohn, P. W. Ion Accumulation and Migration Effects on Redox Cycling in Nanopore Electrode Arrays at Low Ionic Strength. *ACS Nano* **2016**, *10* (3), 3658–3664. https://doi.org/10.1021/acsnano.6b00049.

(30) Freedman, K. J.; Otto, L. M.; Ivanov, A. P.; Barik, A.; Oh, S.-H.; Edel, J. B. Nanopore Sensing at Ultra-Low Concentrations Using Single-Molecule Dielectrophoretic Trapping. *Nat Commun* **2016**, *7* (1), 10217. https://doi.org/10.1038/ncomms10217.

(31) Jaugstetter, M.; Blanc, N.; Kratz, M.; Tschulik, K. Electrochemistry under Confinement. *Chem. Soc. Rev.* **2022**, *51* (7), 2491–2543. https://doi.org/10.1039/D1CS00789K.

(32) Fu, K.; Han, D.; Crouch, G. M.; Kwon, S.-R.; Bohn, P. W. Voltage-Gated Nanoparticle Transport and Collisions in Attoliter-Volume Nanopore Electrode Arrays. *Small* **2018**, *14* (18), 1703248. https://doi.org/10.1002/smll.201703248.

(33) Branagan, S. P.; Contento, N. M.; Bohn, P. W. Enhanced Mass Transport of Electroactive Species to Annular Nanoband Electrodes Embedded in Nanocapillary Array Membranes. *J. Am. Chem. Soc.* **2012**, *134* (20), 8617–8624. https://doi.org/10.1021/ja3017158.

(34) Goines, S.; Dick, J. E. Review—Electrochemistry's Potential to Reach the Ultimate Sensitivity in Measurement Science. *J. Electrochem. Soc.* **2019**, *167* (3), 037505. https://doi.org/10.1149/2.0052003JES.

(35) Weiß, L. J. K.; Music, E.; Rinklin, P.; Straumann, L.; Grob, L.; Mayer, D.; Wolfrum, B. Engineering Electrostatic Repulsion of Metal Nanoparticles for Reduced Adsorption in Single-Impact Electrochemical Recordings. *ACS Appl. Nano Mater.* **2021**, *4* (8), 8314–8320. https://doi.org/10.1021/acsanm.1c01507.

(36) Weiß, L. J. K.; Music, E.; Rinklin, P.; Straumann, L.; Grob, L.; Mayer, D.; Wolfrum, B. Engineering Electrostatic Repulsion of Metal Nanoparticles for Reduced Adsorption in Single-Impact Electrochemical Recordings. *ACS Appl. Nano Mater.* **2021**, *4* (8), 8314–8320. https://doi.org/10.1021/acsanm.1c01507.

(37) Ngamchuea, K.; Clark, R. O. D.; Sokolov, S. V.; Young, N. P.; Batchelor-McAuley, C.; Compton, R. G. Single Oxidative Collision Events of Silver Nanoparticles: Understanding the Rate-Determining Chemistry. *Chem. Eur. J.* **2017**, *23* (63), 16085–16096. https://doi.org/10.1002/chem.201703591.

(38) Krause, K. J.; Brings, F.; Schnitker, J.; Kätelhön, E.; Rinklin, P.; Mayer, D.; Compton, R. G.; Lemay, S. G.; Offenhäusser, A.; Wolfrum, B. The Influence of Supporting Ions on the Electrochemical Detection of Individual Silver Nanoparticles: Understanding the Shape and Frequency of Current Transients in Nano-Impacts. *Chem. Eur. J.* **2017**, *23* (19), 4638–4643. https://doi.org/10.1002/chem.201605924.

(39) Kulkarni, A.; Siahrostami, S.; Patel, A.; Nørskov, J. K. Understanding Catalytic Activity Trends in the Oxygen Reduction Reaction. *Chem. Rev.* **2018**, *118* (5), 2302–2312. https://doi.org/10.1021/acs.chemrev.7b00488.

(40) Ge, X.; Sumboja, A.; Wuu, D.; An, T.; Li, B.; Goh, F. W. T.; Hor, T. S. A.; Zong, Y.; Liu, Z. Oxygen Reduction in Alkaline Media: From Mechanisms to Recent Advances of Catalysts. *ACS Catal.* **2015**, *5* (8), 4643–4667. https://doi.org/10.1021/acscatal.5b00524.

(41) Dau, H.; Limberg, C.; Reier, T.; Risch, M.; Roggan, S.; Strasser, P. The Mechanism of Water Oxidation: From Electrolysis via Homogeneous to Biological Catalysis. *ChemCatChem* **2010**, *2* (7), 724–761. https://doi.org/10.1002/cctc.201000126.

(42) Lyklema, J. Solid-Liquid Interfaces. In *Fundamentals of Interface and Colloid Science*; Elsevier, 1995; Vol. 2. https://doi.org/10.1016/S1874-5679(06)80006-1.

(43) Gu, Y.; Li, D. The ζ-Potential of Glass Surface in Contact with Aqueous Solutions. *Journal of Colloid and Interface Science* **2000**, *226* (2), 328–339. https://doi.org/10.1006/jcis.2000.6827.

(44) Robinson, D. A.; Kondajji, A. M.; Castañeda, A. D.; Dasari, R.; Crooks, R. M.; Stevenson, K. J. Addressing Colloidal Stability for Unambiguous Electroanalysis of Single Nanoparticle Impacts. *J. Phys. Chem. Lett.* **2016**, *7* (13), 2512–2517. https://doi.org/10.1021/acs.jpclett.6b01131.

(45) Zhang, Y.; Robinson, D. A.; McKelvey, K.; Ren, H.; White, H. S.; Edwards, M. A. A High-Pressure System for Studying Oxygen Reduction During Pt Nanoparticle Collisions. *J. Electrochem. Soc.* **2020**, *167* (16), 166507. https://doi.org/10.1149/1945-7111/abcde2.

(46) Kline, T. R.; Iwata, J.; Lammert, P. E.; Mallouk, T. E.; Sen, A.; Velegol, D. Catalytically Driven Colloidal Patterning and Transport. *J. Phys. Chem. B* **2006**, *110* (48), 24513–24521. https://doi.org/10.1021/jp064393l.

(47) Karimi, A.; Kirk, K. A.; Andreescu, S. Electrochemical Investigation of PH-Dependent Activity of Polyethylenimine-Capped Silver Nanoparticles. *ChemElectroChem* **2017**, *4* (11), 2801–2806. https://doi.org/10.1002/celc.201700460.

(48) Chen, W.; Wang, H.; Tang, H.; Yang, C.; Li, Y. Unique Voltammetry of Silver Nanoparticles: From Single Particle to Aggregates. *Anal. Chem.* **2019**, *91* (22), 14188–14191. https://doi.org/10.1021/acs.analchem.9b03372.

(49) Wonner, K.; Rurainsky, C.; Tschulik, K. Operando Studies of the Electrochemical Dissolution of Silver Nanoparticles in Nitrate Solutions Observed With Hyperspectral Dark-Field Microscopy. *Frontiers in Chemistry* **2020**, *7*, 912. https://doi.org/10.3389/fchem.2019.00912.

(50) Fernando, I.; Zhou, Y. Impact of PH on the Stability, Dissolution and Aggregation Kinetics of Silver Nanoparticles. *Chemosphere* **2019**, *216*, 297–305. https://doi.org/10.1016/j.chemosphere.2018.10.122.

(51) Lemineur, J.-F.; Stockmann, T. J.; Médard, J.; Smadja, C.; Combellas, C.; Kanoufi, F. Optical Nanoimpacts of Dielectric and Metallic Nanoparticles on Gold Surface by Reflectance Microscopy: Adsorption or Bouncing? *J. Anal. Test.* **2019**, *3* (2), 175–188. https://doi.org/10.1007/s41664-019-00099-8.

(52) Golestanian, R.; Liverpool, T. B.; Ajdari, A. Designing Phoretic Micro- and Nano-Swimmers. *New J. Phys.* **2007**, *9* (5), 126–126. https://doi.org/10.1088/1367-2630/9/5/126.

(53) Ha, D.; Seo, S.; Lee, K.; Kim, T. Dynamic Transport Control of Colloidal Particles by Repeatable Active Switching of Solute Gradients. *ACS Nano* **2019**, *13* (11), 12939–12948. https://doi.org/10.1021/acsnano.9b05507.

(54) Silvera Batista, C. A.; Rezvantalab, H.; Larson, R. G.; Solomon, M. J. Controlled Levitation of Colloids through Direct Current Electric Fields. *Langmuir* **2017**, *33* (41), 10861–10867. https://doi.org/10.1021/acs.langmuir.7b00835.

(55) Kar, A.; Chiang, T.-Y.; Ortiz Rivera, I.; Sen, A.; Velegol, D. Enhanced Transport into and out of Dead-End Pores. *ACS Nano* **2015**, *9* (1), 746–753. https://doi.org/10.1021/nn506216b.

(56) Lee, K.; Lee, J.; Ha, D.; Kim, M.; Kim, T. Low-Electric-Potential-Assisted Diffusiophoresis for Continuous Separation of Nanoparticles on a Chip. *Lab Chip* **2020**, *20* (15), 2735–2747. https://doi.org/10.1039/D0LC00196A.

(57) Feldmann, D.; Maduar, S. R.; Santer, M.; Lomadze, N.; Vinogradova, O. I.; Santer, S. Manipulation of Small Particles at Solid Liquid Interface: Light Driven Diffusioosmosis. *Sci Rep* **2016**, *6* (1), 36443. https://doi.org/10.1038/srep36443.

(58) Yalcin, S. E.; Lee, S. Y.; Joo, S. W.; Baysal, O.; Qian, S. Electrodiffusiophoretic Motion of a Charged Spherical Particle in a Nanopore. *J. Phys. Chem. B* **2010**, *114* (11), 4082–4093. https://doi.org/10.1021/jp100784p.

(59) Marbach, S.; Bocquet, L. Osmosis, from Molecular Insights to Large-Scale Applications. *Chem. Soc. Rev.* **2019**, *48* (11), 3102–3144. https://doi.org/10.1039/C8CS00420J.

(60) Prieve, D. C.; Anderson, J. L.; Ebel, J. P.; Lowell, M. E. Motion of a Particle Generated by Chemical Gradients. Part 2. Electrolytes. *Journal of Fluid Mechanics* **1984**, *148*, 247–269. https://doi.org/10.1017/S0022112084002330.

(61) Tricoli, V.; Orsini, G. Electrodiffusiophoresis of a Large-Zeta-Potential Particle in Weak Fields. *J. Phys.: Condens. Matter* **2015**, *27* (41), 415102. https://doi.org/10.1088/0953-8984/27/41/415102.

(62) Rica, R. A.; Bazant, M. Z. Electrodiffusiophoresis: Particle Motion in Electrolytes under Direct Current. *Physics of Fluids* **2010**, *22* (11), 112109. https://doi.org/10.1063/1.3496976.

(63) Kang, K. H.; Li, D. Force Acting on a Dielectric Particle in a Concentration Gradient by Ionic Concentration Polarization under an Externally Applied DC Electric Field. *Journal of colloid and interface science* **2005**. https://doi.org/10.1016/J.JCIS.2005.01.049.

(64) Keh, H. J. Diffusiophoresis of Charged Particles and Diffusioosmosis of Electrolyte Solutions. *Current Opinion in Colloid & Interface Science* **2016**, *24*, 13–22. https://doi.org/10.1016/j.cocis.2016.05.008.

(65) Wu, J. H.; Keh, H. J. Diffusioosmosis and Electroosmosis in a Capillary Slit with Surface Charge Layers. *Colloids and Surfaces A: Physicochemical and Engineering Aspects* **2003**, *212* (1), 27–42. https://doi.org/10.1016/S0927-7757(02)00289-3.

(66) Sokolov, S. V.; Eloul, S.; Kätelhön, E.; Batchelor-McAuley, C.; Compton, R. G. Electrode–Particle Impacts: A Users Guide. *Phys. Chem. Chem. Phys.* **2017**, *19* (1), 28–43. https://doi.org/10.1039/C6CP07788A.

(67) Shoup, D.; Szabo, A. Chronoamperometric Current at Finite Disk Electrodes. *Journal of Electroanalytical Chemistry and Interfacial Electrochemistry* **1982**, *140* (2), 237–245. https://doi.org/10.1016/0022-0728(82)85171-1.

(68) Squires, T. M.; Messinger, R. J.; Manalis, S. R. Making It Stick: Convection, Reaction and Diffusion in Surface-Based Biosensors. *Nat Biotechnol* **2008**, *26* (4), 417–426. https://doi.org/10.1038/nbt1388.

(69) Defnet, P. A.; Anderson, T. J.; Zhang, B. Stochastic Collision Electrochemistry of Single Silver Nanoparticles. *Current Opinion in Electrochemistry* **2020**, *22*, 129–135. https://doi.org/10.1016/j.coelec.2020.06.004.

(70) Saw, E. N.; Kanokkanchana, K.; Amin, H. M. A.; Tschulik, K. Unravelling Anion Solvation in Water-Alcohol Mixtures by Single Entity Electrochemistry. *ChemElectroChem* **2022**, *9* (7), e202101435. https://doi.org/10.1002/celc.202101435.

(71) Saw, E. N.; Blanc, N.; Kanokkanchana, K.; Tschulik, K. Time-Resolved Impact Electrochemistry - A New Method to Determine Diffusion Coefficients of Ions in Solution. *Electrochimica Acta* **2018**, *282*, 317–323. https://doi.org/10.1016/j.electacta.2018.06.013.

(72) Ahmadinasab, N.; Stockmann, T. J. Single-Entity Electrochemical Detection of As-Prepared Metallic and Dielectric Nanoparticle Stochastic Impacts in a Phosphonium Ionic Liquid. *ChemElectroChem n/a* (n/a), e202200162. https://doi.org/10.1002/celc.202200162.

TOC

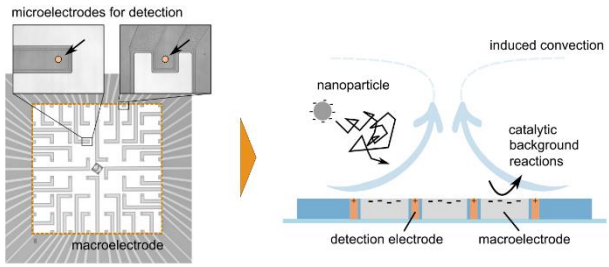
microelectrodes for detection
macroelectrode
induced convection
nanoparticle
catalytic
background
reactions
detection electrode
macroelectrode